Design and Validation of the GA-based Sliding Mode Controller for a Two Degree-of-Freedom Translational Optical Image Stabilizer in Image Sensors

Jeremy H.-S. Wang, Paul C.-P. Chao

Abstract— **This study proposes a genetic algorithm (GA) based sliding mode controller (SMC) for two degree-of-freedom (DOF) translational optical image stabilizer (OIS) of cell cameras installed in the mobile phone. Hand tremors vibrates the lens holder to causes the photographed object projected on different pixels of the image sensor while shooting a picture. The OIS can stabilize the lens holder and efficiently improve the blurring image. The OIS controls a two-DOF translational stage actuated by voice coil motors (VCMs) to stabilize the lens holder for up to four directions of involuntary vibrations. This study includes three main parts: (1) mechanism analysis, (2) establishments of the dynamic equation of motions (EOMs) of the two-DOF translational mechanism, and (3) designs and realizations of a sliding mode controller optimized by genetic algorithm. The first part shows the OIS four-parallel-wire suspension mechanism providing the two-DOF planar movement for the lens holder and magnets offering electro-magnetic force for actuation. In the second part, based on the Lagrange's laws, the dynamics EOMs are derived and analyzed through considering kinetic and potential energy. The last parts include a GA-based SMC is designed to control the lens holder based on EOMs and associated simulations are conducted. According to the simulations, The GA-based SMC is forged and tested by a real-time system integrating a field programmable gate array (FPGA) module. The controllers containing the derived system is built up for anti-shake mechanism. After a series of experiments and verifications, the designed OIS can reduce the vibrations within 5-8 μm in 0.05 seconds. The setting time of experimental results are much less than 0.1 seconds of the previously report and the residual vibration is smaller than the pixel size of the most commercial image sensor. Thus, the prototype of the novel OIS is finally accomplished with satisfactory performance of vibration reduction.**

***Index Terms*—Optical Image Stabilizer, Equations of Motion (EOM), Genetic Algorithm, Sliding Mode Controller.**

I. INTRODUCTION

Image stabilization (IS) technology [1]-[3] has been considered essential to delivering improved image quality in professional cameras. IS also has increasing popular to camera installed in a smart phone. IS is majorly classified into Digital image stabilization (DIS) and Optical image stabilization (OIS) which are applied to improve the image blur. DIS required more memory and computation resource on the host, while OIS directly controls the lens holder position and minimizes memory and computation demands [4]-[8]. OIS also provides better ability to reduce the image blur than OIS [9].

This study is dedicated to develop OIS system that improve the blurring image caused external involuntary vibration. The design and validation of the OIS system include three parts: (1) mechanism designs, (2) establishments of dynamic equation of motion of a two-DOF translational structure, and (3) the design and realization of a SMC with high-precision. The first part focus on the mechanism analysis that the four-parallel-wire suspension structure of the lens holder offers the translational movements along x- and y-direction to reduce the image blur. To stabilized the movement of the lens holder to the desired position for reducing the negative effect by the external involuntary vibration, the behavior of the OIS must be developed a set of equation of motions. Therefore, the second part presents the derivations of EOMs and the analysis of the of the dynamics of the OIS mechanism based on Lagrange's laws. The EOMs are considering the variations of the magnetic force, moments of inertia and the rotation angle and the translational movement of the lens module. The complicated dynamic equations can therefore completely describe the behavior of the OIS lens. The SMC is forged with EOMs in the last part. A series of simulations and experiments are conducted. The performance for several types of shock is tested and the functions of the image stabilization is proven finally.

II. OIS MECHANISM ANALYSIS

The mechanical characteristics of the proposed OIS with two translational DOFs are in small and slim size (only 10.5mm*10.5mm*4mm) and suitable to be installed in a smart phone. The main mechanical structures of the OIS mechanism are shown as Fig. 1. The lens module linked the outer frame with the pattern springs is for image focus. The outer frame attached the four magnets with the opposite pole is supported by four-parallel-wire suspension structure providing two translational DOFs movement of the lens holder. The electro-magnetic force between the magnets and coils located the image base is controlled to actuate the lens holder. All the characteristics of the OIS system are listed on

Jeremy H.-S. Wang, Institute of Electrical and Control Engineering, National Chiao Tung University, Hsinchu city 300, Taiwan, Mobile No.:+886-5131477.

Paul C.-P. Chao, Institute of Electrical and Control Engineering, National Chiao Tung University, Hsinchu city 300, Taiwan, Mobile No.:+886-5131477.

Table 1.

To control the movement of the lens holder to eliminate the hand tremors, the electromagnetic force generated by VCMs pushes the lens holder in the opposite direction of the impulse shock. Based on the electromagnetic theory, the generating force can be determined as

$$\boldsymbol{F} = N \cdot \boldsymbol{i} \cdot L \times \boldsymbol{B}_g. \quad (1)$$

N is the number of coil loops of a VCM, $\boldsymbol{i}$ is the VCM current, L is the total length wire, and $\boldsymbol{B}_g$ is the magnetic flux density that results from geometric design of magnets and shield case.

The Vibrated lens diverges the collimated incident ray projecting on the image sensor while shooting a picture. To reduce the vibration of the lens holder, the GA-Based sliding mode controller is based on the electromagnetic theory and the below the dynamic equations to compute the magnitude of the VCM current to generate the electromagnetic force to move the lens holder supported by four-wire suspension according to the measurements acquired by the gyroscope and accelerometer. Thus, the controlled planar movement of the lens holder can keep stabilized relative to the photographed object and the OIS improves the blur picture.

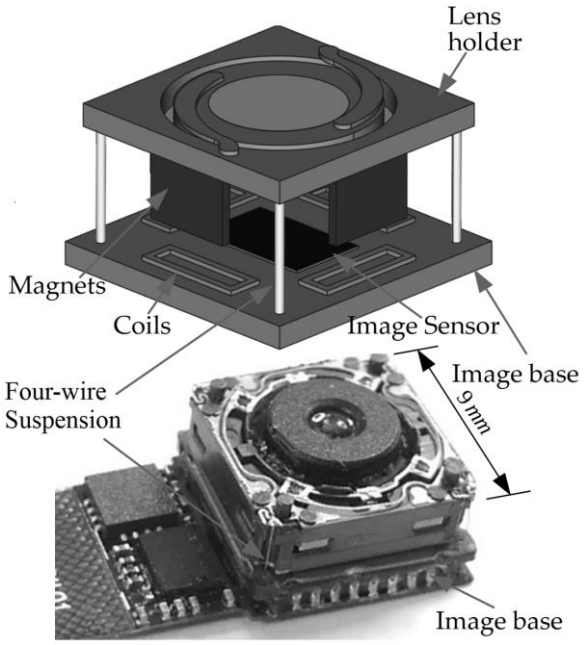

Figure 1. Optical image structure. Main structure consists of lens holder supported by four-parallel wires on the image base, coils and magnets.

Table 1. Specifications of optical image stabilizer.

Item	Specifications
Lens holder Diameter	9mm
Lens holder weight	0.5202g
Rated Load Current	80mA
Working range	±1mm
Moving displacement	±1mm
OIS Dimensions	105mm*10.5mm*4mm

III. Derivation and Analysis of Dynamic Equations for OIS

The equations of motion are shown in this section. Based on Lagrange's laws, the dynamics equations are derived and analyzed by considering the kinetic and potential energy. Define $X_gY_gZ_g$ as an inertial reference frame whose origin is O_g and $X_gY_gZ_g$ symbolizes the ground reference coordinates. In addition to $X_gY_gZ_g$, there are two other coordinate system, $X_iY_iZ_i$ and $X_lY_lZ_l$, which are fixed at the image base and the lens holder, respectively. The coordinates and notations are described in Fig. 2. The hand tremor causes three translational movements and three rotations. Thus, the acceleration and the angular acceleration of O_i can be expressed as (2), respectively.

$$a_{o_i} = \ddot{x}_i\hat{\imath} + \ddot{y}_i\hat{\jmath} + \ddot{z}_i\hat{k}. \quad \ddot{\theta}_{o_i} = \ddot{\theta}_{x_i}\hat{\imath} + \ddot{\theta}_{y_i}\hat{\jmath} + \ddot{\theta}_{z_i}\hat{k}. \quad (2)$$

a_{o_i} and $\ddot{\theta}_{o_i}$ stand for the sensor measurements in the translational and angular motion, respectively. And the lens holder often slightly rotates along z axis. θ_{z_l} does the rotational angle between $X_iY_iZ_i$ and $X_lY_lZ_l$, i.e. the roll angle, as Fig. 2(b). Thus, the transform matrix exists between $X_iY_iZ_i$ and $X_lY_lZ_l$ as (3).

$$T = \begin{bmatrix} cos\theta_{z_l} & sin\theta_{z_l} & 0 \\ -sin\theta_{z_l} & cos\theta_{z_l} & 0 \\ 0 & 0 & 1 \end{bmatrix}. \quad (3)$$

While the motion of the lens holder in a non-inertial frame of reference, Lagrange's equations [10]-[12] are shown as

$$L = \frac{1}{2}mv^2 + m\boldsymbol{v} \cdot \boldsymbol{\Omega} \times \boldsymbol{r} + \frac{1}{2}m(\boldsymbol{\Omega} \times \boldsymbol{r})^2 - m\boldsymbol{W} \cdot \boldsymbol{r} - U, \quad (4)$$

where $\boldsymbol{r}$ is the displacement, $\boldsymbol{v}$ is the velocity, $\boldsymbol{\Omega}$ is angular velocity of the lens holder relative to the image base. $\boldsymbol{W}$ stands for acceleration of the image base in $X_gY_gZ_g$. L and U is kinetic energy and potential energy, respectively. Therefore, $\boldsymbol{r}$, $\boldsymbol{v}$, $\boldsymbol{\Omega}$, and $\boldsymbol{W}$ for a given point (dm) in Fig. 2 can represent as

$$\boldsymbol{r} = (x_l + x_{dm}cos\theta_{z_l} - y_{dm}\sin\theta_{z_l})\hat{\imath} + (y_l + x_{dm}sin\theta_{z_l} + y_{dm}cos\theta_{z_l})\hat{\jmath} + (z_l + z_{dm})\hat{k}, \quad (5)$$

$$\boldsymbol{v} = (\dot{x}_l - \dot{\theta}_{z_l}x_{dm}sin\theta_{z_l} - \dot{\theta}_{z_l}y_{dm}cos\theta_{z_l})\hat{\imath} + (\dot{y}_l + \dot{\theta}_{z_l}x_{dm}cos\theta_{z_l} - y_{dm}sin\theta_{z_l})\hat{\jmath} + \dot{z}_l\hat{k}, \quad (6)$$

$$\boldsymbol{\Omega} = \dot{\theta}_{x_i}\hat{\imath} + \dot{\theta}_{y_i}\hat{\jmath} + \dot{\theta}_{z_i}\hat{k}, \quad (7)$$

$$\boldsymbol{W} = \ddot{x}_i\hat{\imath} + \ddot{y}_i\hat{\jmath} + \ddot{z}_i\hat{k}. \quad (8)$$

The kinetic energy and potential energy for the lens holder can be shown as below equations, respectively.

$$E_k = \int \left(\frac{1}{2}v^2 + \boldsymbol{v} \cdot \boldsymbol{\Omega} \times \boldsymbol{r} + \frac{1}{2}(\boldsymbol{\Omega} \times \boldsymbol{r})^2 - \boldsymbol{W} \cdot \boldsymbol{r}\right) dm, \quad (9)$$

$$U = \frac{1}{2}k(x_l^2 + y_l^2) + \frac{1}{2}k_\theta\theta_{z_l}^2 + gy_lm. \quad (10)$$

Substituting (5)-(8) into (9), the equations of motion can be readily obtained as (11)-(13) according to Lagrange's laws.

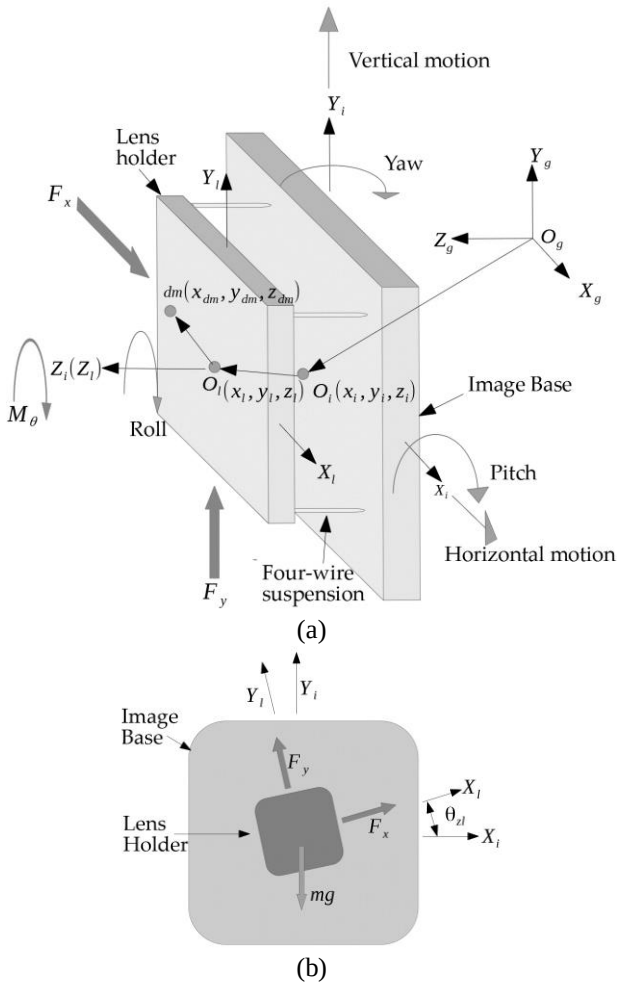

Figure 2. Coordinates and notations of the OIS model. (**a**) 3-D view; (**b**) Electromagnetic forces on the centroid of the lens holder.

$$(\ddot{x}_i + \ddot{x}_l - \dot{\theta}_{y_i}^2 x_l - \dot{\theta}_{z_i}^2 x_l + \ddot{\theta}_{y_i} z_l - \ddot{\theta}_{z_i} y_l + \dot{\theta}_{x_i}\dot{\theta}_{z_i} z_l + \dot{\theta}_{x_i}\dot{\theta}_{y_i} y_l + 2\dot{\theta}_{y_i}\dot{z}_l - 2\dot{\theta}_{z_i}\dot{y}_l)m + (\dot{\theta}_{x_i}\dot{\theta}_{z_i} + \ddot{\theta}_{y_i})I_z + (\dot{\theta}_{x_i}\dot{\theta}_{y_i} - \ddot{\theta}_{z_i} - \ddot{\theta}_{z_l})(I_x sin\theta_{z_l} + I_y cos\theta_{z_l}) - \left[\dot{\theta}_{y_i}^2 + (\dot{\theta}_{z_i} + \dot{\theta}_{z_l})^2\right](I_x cos\theta_{z_l} - I_y sin\theta_{z_l}) = F_x cos\theta_{z_l} - F_y sin\theta_{z_l} - k_x x_l - c_x \dot{x}_l, \quad (11)$$

$$(\dot{y}_i + \ddot{y}_l - \dot{\theta}_{x_i}^2 y_l - \dot{\theta}_{z_i}^2 y_l + \ddot{\theta}_{z_i} x_l - \ddot{\theta}_{x_i} z_l + \dot{\theta}_{y_i}\dot{\theta}_{z_i} z_l + \dot{\theta}_{x_i}\dot{\theta}_{y_i} x_l + 2\dot{\theta}_{z_i}\dot{x}_l - 2\dot{\theta}_{x_i}\dot{z}_l)m + (\dot{\theta}_{y_i}\dot{\theta}_{z_i} - \ddot{\theta}_{x_i})I_z - \left[\dot{\theta}_{x_i}^2 + (\dot{\theta}_{z_i} + \dot{\theta}_{z_l})^2\right](I_x sin\theta_{z_l} + I_y cos\theta_{z_l}) + (\ddot{\theta}_{z_i} + \ddot{\theta}_{z_l} + \dot{\theta}_{x_i}\dot{\theta}_{y_i})(I_x cos\theta_{z_l} - I_y sin\theta_{z_l}) = F_y cos\theta_{z_l} + F_x sin\theta_{z_l} - k_y y_l - c_y \dot{y}_l - mg, \quad (12)$$

$$(I_x cos\theta_{z_l} - I_y sin\theta_{z_l})(\ddot{y}_i + \ddot{y}_l - \dot{\theta}_{x_i}^2 y_l - \dot{\theta}_{z_i}^2 y_l + \ddot{\theta}_{z_i} x_l - \ddot{\theta}_{x_i} z_l + \dot{\theta}_{y_i}\dot{\theta}_{z_i} z_l + \dot{\theta}_{x_i}\dot{\theta}_{y_i} x_l + 2\dot{\theta}_{z_i}\dot{x}_l - 2\dot{\theta}_{x_i}\dot{z}_l) - (I_x sin\theta_{z_l} + I_y cos\theta_{z_l})(\ddot{x}_i + \ddot{x}_l - \dot{\theta}_{y_i}^2 x_l - \dot{\theta}_{z_i}^2 x_l + \ddot{\theta}_{y_i} z_l - \ddot{\theta}_{z_i} y_l + \dot{\theta}_{x_i}\dot{\theta}_{z_i} z_l + \dot{\theta}_{x_i}\dot{\theta}_{y_i} y_l + 2\dot{\theta}_{y_i}\dot{z}_l - 2\dot{\theta}_{z_i}\dot{y}_l) + (I_{xz}\cos\theta_{z_l} - I_{yz} sin\theta_{z_l})(\dot{\theta}_{y_i}\dot{\theta}_{z_i} - \ddot{\theta}_{x_i}) - (I_{xz} sin\theta_{z_l} + I_{yz} cos\theta_{z_l})(\dot{\theta}_{x_i}\dot{\theta}_{z_i} + \ddot{\theta}_{y_i}) + (\dot{\theta}_{y_i}^2 - \dot{\theta}_{x_i}^2)(I_{xx}\sin\theta_{z_l}\cos\theta_{z_l} + I_{xy}(\cos^2\theta_{z_l} - \sin^2\theta_{z_l}) - I_{yy}\cos\theta_{z_l}\sin\theta_{z_l}) + (\ddot{\theta}_{z_i} + \ddot{\theta}_{z_l})I_\theta + \dot{\theta}_{x_i}\dot{\theta}_{y_i}(I_{xx}\cos^2\theta_{z_l} + I_{yy}\sin^2\theta_{z_l} - 2I_{xy}\sin\theta_{z_l}\cos\theta_{z_l}) - \dot{\theta}_{x_i}\dot{\theta}_{y_i}(I_{xx}\sin^2\theta_{z_l} + I_{yy}\cos^2\theta_{z_l} + 2I_{xy}\sin\theta_{z_l}\cos\theta_{z_l}) = M_\theta - k_\theta\theta_{z_l} - c_\theta\dot{\theta}_{z_l}, \quad (13)$$

where x, y, z, θ_x, θ_y and θ_z do the translational and rotational motions in x-, y- and z-axis, respectively. The suffixes (i and l) symbolize the image base and the lens holder, respectively. I_{xx}, I_{yy} and I_θ are the mass moment of inertia of the lens holder and I_{xy}, I_{xz}, are the mass product of inertia of the lens holder about its centroid along the x-, y- and z-axis, respectively, while $I_x = \int_m x_{dm}\, dm$ and $I_y = \int_m y_{dm}\, dm$ are first mass moments of inertia with respect to the x- and y-axes, respectively. k_x, k_y and $k_\theta$of four-wire suspension structure are the equivalent spring stiffness in x-, y- and roll-axis, respectively. c_x, c_y and c_θ of four-wire suspension structure are the equivalent spring damping coefficient in x-, y- and roll-axis, respectively. F_x, F_y and M_θ are the force and moment for actuation, respectively. Note that k_x equals k_y, c_x equals c_y and I_{xx} equals I_{yy} due to the nearly symmetric structure.

Because of the lens holder is the symmetric structure, the mass product of inertia and the first mass moments of inertia are very small and negligible. The distance (z_l) between the image base and lens holder is constant due to the four-parallel-wire structure. Thus, terms, $\dot{z}_l$ and $\ddot{z}_l$, are eliminated in (11)-(13). Thus, the dynamics equations are rearranged as

$$m\ddot{x}_l + m\ddot{x}_i + c_x\dot{x}_l + k_x x_l - m(\dot{\theta}_{y_i}^2 + \dot{\theta}_{z_i}^2)x_l - 2m\dot{\theta}_{z_i}\dot{y}_l + m(\dot{\theta}_{x_i}\dot{\theta}_{y_i} - \ddot{\theta}_{z_i})y_l + m(\dot{\theta}_{x_i}\dot{\theta}_{z_i} + \ddot{\theta}_{y_i})z_l = F_x cos\theta_{z_l} - F_y sin\theta_{z_l}, \quad (14)$$

$$m\ddot{y}_l + m\ddot{y}_i + 2m\dot{\theta}_{z_i}\dot{x}_l + m(\ddot{\theta}_{z_i} + \dot{\theta}_{x_i}\dot{\theta}_{y_i})x_l + c_y\dot{y}_l - m(\dot{\theta}_{x_i}^2 + \dot{\theta}_{z_i}^2)y_l + k_y y_l + +m(\dot{\theta}_{y_i}\dot{\theta}_{z_i} - \ddot{\theta}_{x_i})z_l = F_y cos\theta_{z_l} + F_x\theta_{z_l}, \quad (15)$$

$$(\ddot{\theta}_{z_i} + \ddot{\theta}_{z_l})I_\theta + c_\theta\dot{\theta}_{z_l} + k_\theta\theta_{z_l} = M_\theta. \quad (16)$$

Only the variation of θ_{z_l}, the angle in roll direction, cannot change image point on the image sensor because of the symmetric circular sharp of the lens. In addition, θ_{z_l} is very small due to the nation of the four parallel wires. Therefore, (14) and (15) are considered to forge a controller to reduce image blur, ignoring the motion in an addition DOF of roll. Finally, the dynamic equations of the 2-DOF translational OIS are obtain as follow.

$$M\ddot{q}_l + M\ddot{q}_i + C\dot{q}_l + Kq_l + N + G = TF, \quad (17)$$

$$M = diag[m \quad m], \quad (18)$$

$$C = \begin{bmatrix} c_x & -2m\dot{\theta}_{z_i} \\ 2m\dot{\theta}_{z_i} & c_y \end{bmatrix}, \quad (19)$$

$$K = \begin{bmatrix} k_x - m(\dot{\theta}_{y_i}^2 - \dot{\theta}_{z_i}^2) & m(\dot{\theta}_{x_i}\dot{\theta}_{y_i} - \ddot{\theta}_{z_i}) \\ m(\ddot{\theta}_{z_i} + \dot{\theta}_{x_i}\dot{\theta}_{y_i}) & k_y - m(\dot{\theta}_{x_i}^2 + \dot{\theta}_{z_i}^2) \end{bmatrix}. \quad (20)$$

$$N = \begin{bmatrix} m(\dot{\theta}_{x_i}\dot{\theta}_{z_i} + \ddot{\theta}_{y_i})z_l \\ m(\dot{\theta}_{y_i}\dot{\theta}_{z_i} - \ddot{\theta}_{x_i})z_l \end{bmatrix}, \quad (21)$$

$$T = \begin{bmatrix} 1 & -\theta_{z_l} \\ \theta_{z_l} & 1 \end{bmatrix}. \quad (22)$$

where $q_i = [x_i \quad y_i]^T$ and $q_l = [x_l \quad y_l]^T$ contain the generalized coordinates standing for the motions of image base and the lens holder, respectively. C, K and M are overall damping coefficient and Coriolis force terms, spring stiffness and mass matrices, N contains the centrifugal force

terms, $G = [0 \quad mg]^T$ captures the gravitational effect, and $F = [F_x \quad F_y]^T$ stands for electromagnetic force for actuation. Equation (17)-(22) includes nonlinear terms and linear terms of EOMs. Thus, (17)-(22) can be re-arranged to nominal terms, the lumped uncertainty terms and nonlinearity terms as (23).

$$M_o\ddot{q}_l + M_o\ddot{q}_i + C_o\dot{q}_l + K_o q_l + \Delta\left(\ddot{q}_l, \dot{q}_l, q_l, \ddot{\theta}_{x_i}, \ddot{\theta}_{y_i}, \dot{\theta}_{x_i}, \dot{\theta}_{y_i}, \dot{\theta}_{z_i}\right) + G = TF, \quad (23)$$

The terms are denoted nominal terms by subscript "o" and $\Delta\left(\ddot{q}_l, \dot{q}_l, q_l, \ddot{\theta}_{x_i}, \ddot{\theta}_{y_i}, \dot{\theta}_{x_i}, \dot{\theta}_{y_i}, \dot{\theta}_{z_i}\right)$ defines the lumped uncertainty due to the model.

$$\Delta\left(\ddot{q}_l, \dot{q}_l, q_l, \ddot{\theta}_{x_i}, \ddot{\theta}_{y_i}, \dot{\theta}_{x_i}, \dot{\theta}_{y_i}, \dot{\theta}_{z_i}\right) = \Delta M\ddot{q}_l + \Delta C\dot{q}_l + \Delta K q_l + N, \quad (24)$$

where $\Delta M = M - M_o$, $\Delta C = C - C_o$ and $\Delta K = K - K_o$. The uncertainty is boundary by following property.

$$\Delta\left(\ddot{q}_l, \dot{q}_l, q_l, \ddot{\theta}_{x_i}, \ddot{\theta}_{y_i}, \dot{\theta}_{x_i}, \dot{\theta}_{y_i}, \dot{\theta}_{z_i}\right) < \delta. \quad (25)$$

IV. Design of Sliding Mode Controller for OIS

A. Control Objectives

Hand tremor causes six-DOF motions (three displacements and three rotations). According to geometric optics, the translational and angular hand tremor in z- and roll direction doesn't causes the blurred picture because the lens cannot diverge the collimated incident light projecting on the image sensor. Thus, the hand tremors in x-, y-, θ_x- and θ_y-axis are considered to derive to control objectives of the lens holder in Fig. 3.

The basic principle underlying OIS is simplified in Fig. 4, where the movement effects are amplified and represented on a single axis for the sake of clarity [13], [14]. Fig. 4(a), (b) indicates the motion of the imaging pointer under the hand tremor along x-, y-, θ_x- and θ_y-axis, respectively. In Fig. 4(a), a downward movement of the camera causes the original imaged point B shifted to B'. Thus, the involuntary tremor causes a blurred image. To improve the blurred image, the lens holder moves opposite to the direction of the translational shock to re-image point B' back to origin B. In case of rotational shock, point B shifted to the under optical axis due to counterclockwise hand tremor. Thus, the lens holder moves upward to re-image point B to B', as shown in Fig. 4(b).

Fig. 5 shows the lens structures simplified as a spherical double-convex single lens. Collimated incident light of the photographed object, A, projects on the image sensor. While camera shaken downward, the shift of A, Δh, causes that the projection, B, on the image sensor moves from h_b to h_b' The relevant equations are as

$$\Delta h\frac{L_b}{L_a} = (h_a + \Delta h)\frac{L_b}{L_a} - h_a\frac{L_b}{L_a} = h_b' - h_b, \quad (26)$$

which yields

$$\Delta h\frac{L_b}{L_a} = \Delta h^*. \quad (27)$$

The gain, $\frac{L_b}{L_a}$, is decided by the focal length. For the sake of clarity, assume that L_a equals L_b. The relative equation between Δh and Δh^* is rearranged as

$$\Delta h \approx \Delta h^*. \quad (28)$$

In other words, the lens movement is equivalent to the displacement of the light ray projecting on an image sensor. Note that the control objective in (28) is equivalent to moving the lens in OIS exactly opposite to the movement of the camera due to hand shaking. For small angular hand tremor in pitch and yaw axes, the compensation movements are equivalent to the magnitude of product of the rotated angle of the vibration and the distance between the lens holder and the image sensor, as shown in Fig. 4(b)

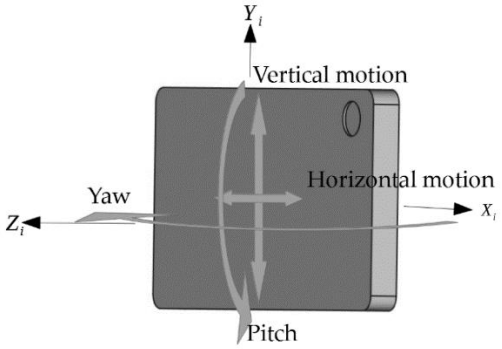

Figure 3. The hand tremors in x-, y-, θ_x- and θ_y-axis.

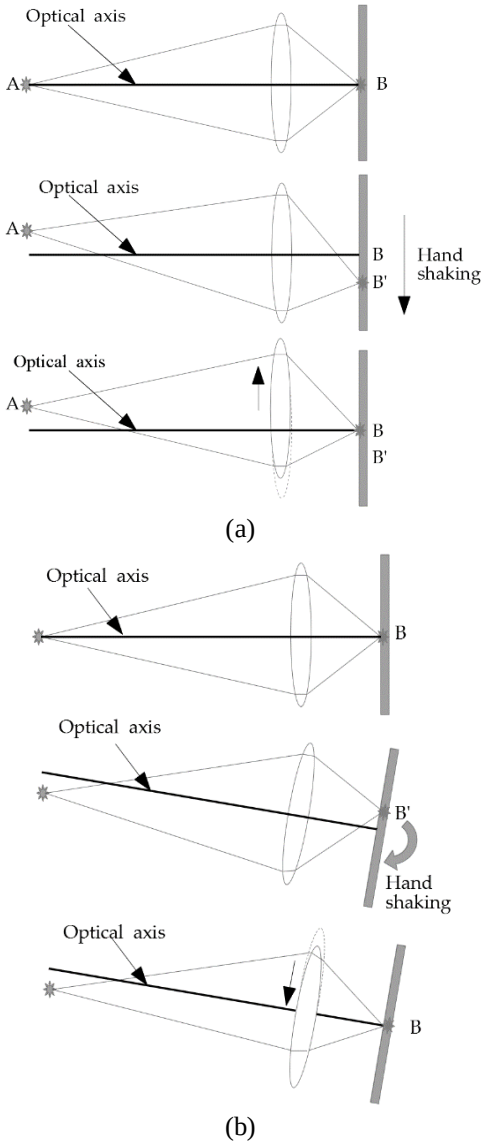

Figure 4. The optical working principles of OIS. (**a**) under

translational disturbance; (**b**)under rotational disturbance.

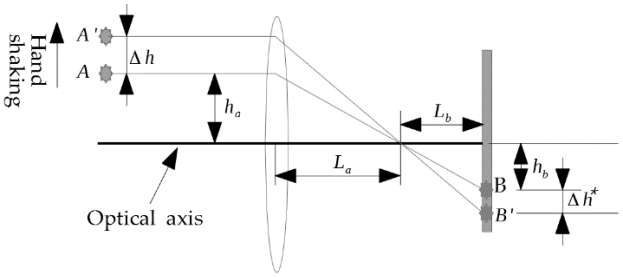

Figure 5. Desired movement of lens holder to compensate for the image blur caused by hand shaking.

B. Design of A Sliding Mode Controller integrated Genetic Algorithm

A traditional sliding mode controller [16]-[18] is proposed to achieve robust performance against parameter variations and external involuntary vibration. But the experience shows the equivalent control law cannot guarantee the performance, especially if the system parameters are perturbed or unknown [19]. Therefore, SMC parameters is obtained by using GA optimization technique [20]-[25]. According to SMC theory, any errors converge to zero while any states approach to the sliding surface.

The desired earth-fixed coordinate defined as $q_d = [x_d \quad y_d \quad z_d \quad \theta_{x_d} \quad \theta_{y_d} \quad \theta_{z_d}]^T$ stands for the photographed object and is stationary. Let the earth-fixed coordinate error denotes by $e = q_d - (q_i + q_l)$ and the sliding surface is express as below:

$$s = \dot{e} + \alpha e. \tag{29}$$

Lyapunov function and the time derivative for x-direction can be written as

$$V_x(t) = \frac{1}{2} m s_x^2, \tag{30}$$

$$\dot{V}_x(t) = m s_x \dot{s}_x. \tag{31}$$

With $q_d = 0$, $\dot{q}_d = 0$, $\ddot{q}_d = 0$ and $m\dot{s}_x = m(\ddot{e}_x + \alpha_x \dot{e}_x)$, $\dot{V}_x(t)$ can be rewritten as follows:

$$\dot{V}_x(t) = -S_x\left[u_x - c_x\dot{x}_l - k_x x_l - \Delta_x\left(\ddot{\theta}_{y_i}, \ddot{\theta}_{z_i}, \dot{\theta}_{x_i}, \dot{\theta}_{y_i}, \dot{\theta}_{z_i}\right) - m_x \alpha_x \dot{e}_x\right], \tag{32}$$

where $u_x = F_x - F_y\theta_{z_l}$. The proposed control u_x is as follow:

$$u_x = \delta_x sat(S_x, \epsilon_x) + \rho_x S_x + c_x\dot{x}_l + k_x x_l + m\alpha_x \dot{e}_x, \tag{33}$$

where $sat(S_x, \epsilon_x) = \frac{S_x}{|S_x| + \epsilon_x}$ for decreasing chatter phenomenon [24], $\epsilon_x > 0$ and $\epsilon_x \approx 0$. u_x is substituted into $\dot{V}_x(t)$ and yields

$$\dot{V}_x = -S_x\left[\delta_x sat(S_x, \epsilon_x) + \rho_s S_x - \Delta_x\left(\ddot{\theta}_{y_i}, \ddot{\theta}_{z_i}, \dot{\theta}_{x_i}, \dot{\theta}_{y_i}, \dot{\theta}_{z_i}\right)\right] \le -\rho_x S_x^2 \le 0. \tag{34}$$

According to (34), control gains, δ_x, ρ_x and α_x, are chosen to be large enough such that $\dot{V}_x(t) < 0$ and it implies $V(t) < V(0)$. Therefore, $s(t)$ is bounded. According to Barbalat's lemma [25], $s(t)$ tending to zero implies the position error converge to the zero exponentially over time. Similarly, the relative equations for y-axis can be expressed as follow:

$$V_y(t) = \tfrac{1}{2} m s_y^2, \ \dot{V}_y(t) = m s_y \dot{s}_y. \tag{35}$$

$$u_y = F_y + F_x\theta_{z_l} = \delta_y sat(S_y, \epsilon_y) + \rho_y S_y + c_y\dot{y}_l + k_y y_l - \alpha_y \dot{e}_y. \tag{36}$$

$$\dot{V}_y = -S_y\left[\delta_y sat(S_y, \epsilon_y) + \rho_y S_y - \Delta_y\left(\ddot{\theta}_{x_i}, \ddot{\theta}_{z_i}, \dot{\theta}_{x_i}, \dot{\theta}_{y_i}, \dot{\theta}_{z_i}\right)\right] \le -\rho_{s_y} S_y^2 \le 0. \tag{37}$$

To select the suitable δ_x, ρ_x and α_x for x-direction and δ_y, ρ_y and α_y for y-direction, respectively, the proposed GA optimizes these parameters for SMC design. The concept of SMC is used to keep the states on the surface $s(t) = 0$ for the all time $t > 0$. Thus, a fitness function [26] based on the sliding surface is defined the following form:

$$FIT(s) = s^2 + 0.1\dot{s}^2, \tag{38}$$

where is a function of the performance index for the sliding surface. Thus, GA finds out the parameters which can minimize the fitness function, i.e., the criterion of $s(t) = 0$ and $\dot{s}(t) = 0$ should be satisfied for the all time $t > 0$. δ, ρ and α of the control forces are presented by a 10-bits binary codes, respectively, which are concatenated together to form 30-bits codes of a chromosome. For simplicity, unsigned binary coding is used and linearity scaled into ranges of the three parameters of control forces. The GA majorly consists of three operators: reproduction, crossover and mutation operators and the main process of proposed GA-based SMC is represented by the following procedures:

1) Select the size of population and fitness function.
2) Generate the initial population standing for gains of SMC and code them into binary string.
3) Evaluate the fitness function via (38) and sort the sequence for the all chromosomes.
4) Select the all chromosomes in the pool for the next step except the smallest and the largest fitness function of the chromosome.
5) Choose the elites for the crossover by the roulette wheel selection based on the fitness function.
6) Crossover pair of members of the elites; Site of crossover is generated randomly.
7) Mutate every binary bit of the chromosomes of the elites according to the mutation probability for the offspring; the mutation probability is not usually select too large to avoid the system dynamic trend to divergence easily.
8) Reproduce the new generation (offspring) from the smallest fitness function of the chromosome of Step 4, a new random chromosome and the preselection chromosomes of Step 7.
9) Iterate on the process between Step 2 and Step 8 the specified times.
10) Compute control forces, u_x and u_y, based on (33) and (36) for OIS, respectively.

C. Work Process For the OIS

With EOMs and control objective successfully derived, the closed-loop system for OIS is ready to synthesize the flowchart of the entire work process illustrated as Fig. 6. While hand tremor occurs, the lens holder, due to its designed supporting structure of four parallel wires, exhibits the planar 2-DOF translational motions for reducing blurred images.

The optics algorithm derived from geometrics optics computes compensating displacement according to the

measurements detected by the gyroscope built into the mobile camera phone. Pulse-width modulation (PWM) signals are used to control the currents of VCM drivers while the sliding mode controller attempts to minimize the error between the desired reference positions and the displacements of the lens holder sensed by the hall sensors attached the image base.

D. System Identification of the OIS

For control design, the OIS model is built by using system identification. While chirp signals from a frequency response analyzer drive the VCMs of the OIS through VCM drivers within the desired frequency range, the frequency response analyzer obtains the voltage signals of the hall sensors indicating the displacement variations relative to the image base over time.

Results of experiments (case a – d) for the OIS system parameter identification are illustrated as Fig. 7. Case (a) and (b) show the frequency response plots of the outputs in x and y directions, respectively, while controlling electromagnetic force in x direction. According to the frequency response plots of case (a) and (b), experiments indicate that the resonance mode of the four-wire parallel structure occurs at a frequency of approximately 57.59 Hz in x direction and the lens holder slightly vibrates simultaneously in y direction. Thus, the structure of the lens holder is very symmetric in roll direction and the spring stiffness of the four parallel wires are close. Case (c) and (d) present the frequency plots in y and x direction while controlling electromagnetic force in y direction. The resonance mode occurs at a frequency of approximately 57.39 Hz and the coupling phenomenon is not also obvious between the electromagnetic force in x direction and the displacement of the lens holder in y direction according to case (d). The resonance frequencies in case (b) and case (d) are like in case(a) and case (c), respectively, because the small angle exists between the sensing direction of the hall sensors and the tracking displacement of the lens holder. So, the first mass moment and mass product of inertia of the lens holder are negligible in EOMs. The spring stiffness and damping coefficient in x and y direction are equivalent according to the resonance frequency in x and y axis, respectively. Table 2 lists the identified parameters of the OIS.

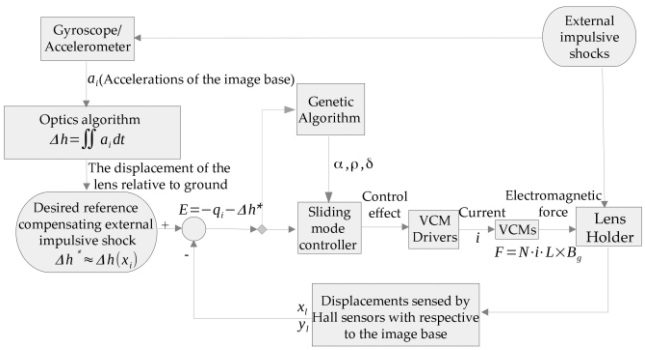

Figure 6. The flowchart of the close-loop system illustrates the entire work.

Table 2. Parameters of Optical image stabilizer.

Item	Specifications
Lens holder mass	0.52202g
Stiffness(k_x) in x axis	67.092N/m
Stiffness(k_y) in y axis	67.081N/m
Stiffness(k_θ) in roll	4.189×10^{-4}N. m
Damping Ratios	0.0577

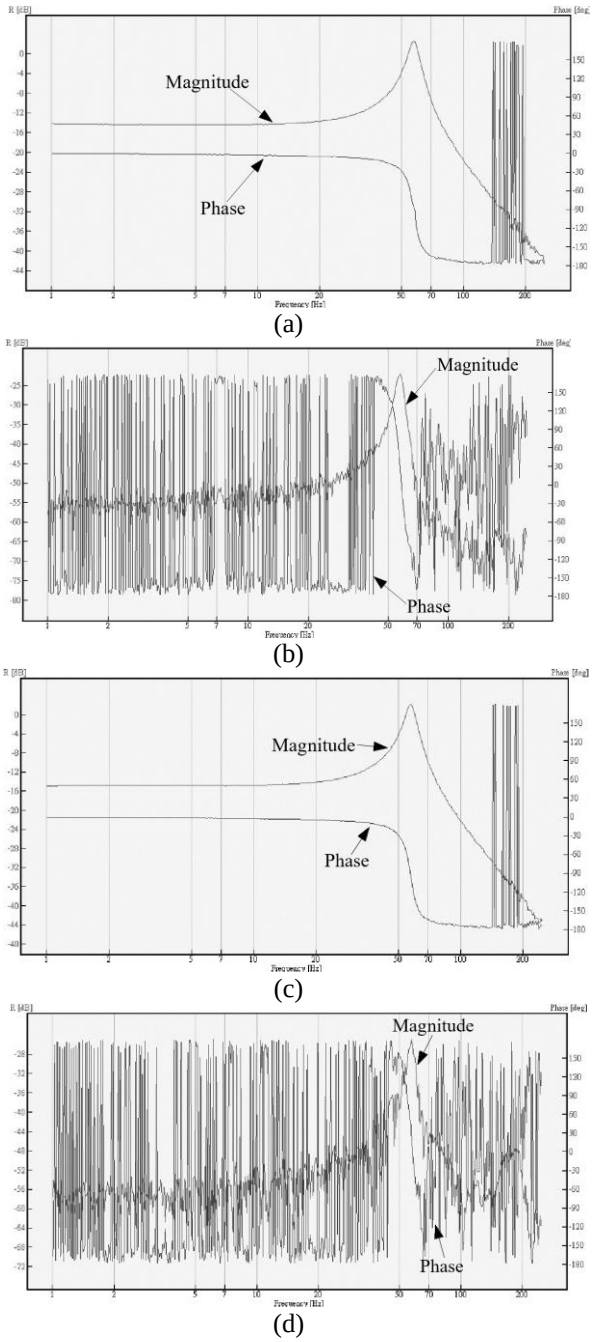

Figure 7. Bode plot of the OIS; (a) Bode plot of the OIS in x-axis while controlling the VCM in x-direction. The resonance frequency occurs at 57.59 Hz; (b) Bode plot of the OIS in y-axis while controlling the VCM in x-direction. the first resonance frequency is at 57.59 Hz; (c) Bode plot of the OIS in y axis while controlling the VCM in y direction. The resonance frequency occurs at 57.39 Hz; (d) Bode plot of the OIS in x axis while controlling the VCM in y direction. the first resonance frequency is at 57.39 Hz.

V. Simulations and Experimental Results

A. Simulations of the GA-based Sliding Mode Controller

To predict preliminary control result is utilized as a simulation tool to estimate a sliding mode controller. The simulation codes are written to realize equations of motion derived in previous sections. The states of angular motion, angular velocities, translational motions, and translational velocities can be obtained with numerical integration. In simulations, harmonics are used to simulates the main natures of the hand shaking. Fig. 8 shows the response simulations of the lens holder at 5 Hz and 10 Hz [13] along x- and y-direction relative to ground, respectively.

From Fig. 8, GA-Based SMC effectively stabilize the lens holder in the range of 3 μm. Note that GA-Based SMC can suppress the coupling effect due to non-zero θ_{z_l} and model uncertainty in (17)-(22), with some degree of robustness. The 3 μm of residual vibration of lens holder is small than the common pixel size of a CCD/CMOS image sensor, which is around 2.4-8.4 μm [27]. Thus, the SMC can meet the requirements of image stabilization, effectively reducing image blurs.

B. Experiments for OIS

To test the performance of the GA-based SMC for stabilizing the lens holder, the experiments case is conducted under differential harmonic signals simulating the common hand shaking. Fig. 9(a) illustrates the experimental setup. Laser displacement sensor is used to measure the movement of the lens holder relative to ground, while stands for the compensated results, as shown in Fig. 9(b). SMC implemented in a real-time FPGA-integrated controller actuates the VCMs of OIS through the VCM driver circuit. The hall sensor built in the image base of OIS is amplified by the hall sensor readout circuit and fed to the real-time FPGA-integrated controller. To verify the experiment results with the aim of reducing the blurring image, a laser displacement sensor is used to measures the motion of lens holder relative to the ground. Thus, while the movement of the image base simulating the external disturbance is generated by the translational 2-DOF shaker in x- and y-direction, the hall sensor and gyroscope immediately measure the movement of the lens holder relative to the image base and the movement of the image base relative to the ground, respectively, and those sensors signals are fed back to SMC. Therefore, according to (36) and (38), the GA-Based SMC regulates the lens holder by VCMs to minimize the error generated by hand shaking. In other words, while hand shaking moves the image base to cause the image blurs, the GA-Based SMC controls the electro-magnetic force, u_x and u_y, to move the lens holder to attenuate the movement of the lens holder relative to ground to effectively reduce the image blurs.

Fig. 10 shows the experiment results while the frequency of the vibration at 5 Hz and 10 Hz along x- and y-axis, respectively. The red line and blue line stand for the external signal and lens holder relative to ground, respectively. The vibrations generated by the shaker at an amplitude of 50 μm at 5 Hz along x- and y-axis of the OIS are reduced to the 6 μm and 7 μm of the resulting residual vibration, which the amplitudes are attenuated to the 12 and 14 percent of the original shock in Fig. 10(a) and 10(b), respectively. Fig. 10(c) and 10(d) presents that external shock of 50 μm at 10 Hz along x- and y-axis of the OIS are attenuated the 5 μm and 8 μm of the resulting residual vibration, which the amplitudes are reduced to the 10 and 16 percent, respectively. The setting time of experimental results is 0.05 seconds and it is better than prior study [7] with result of around 0.1 seconds. Clearly, the GA-based SMC can efficiently stabilize the lens holder affected by the external tremor on optical image stabilization in a general mobile phone camera, significantly eliminate the image blurs

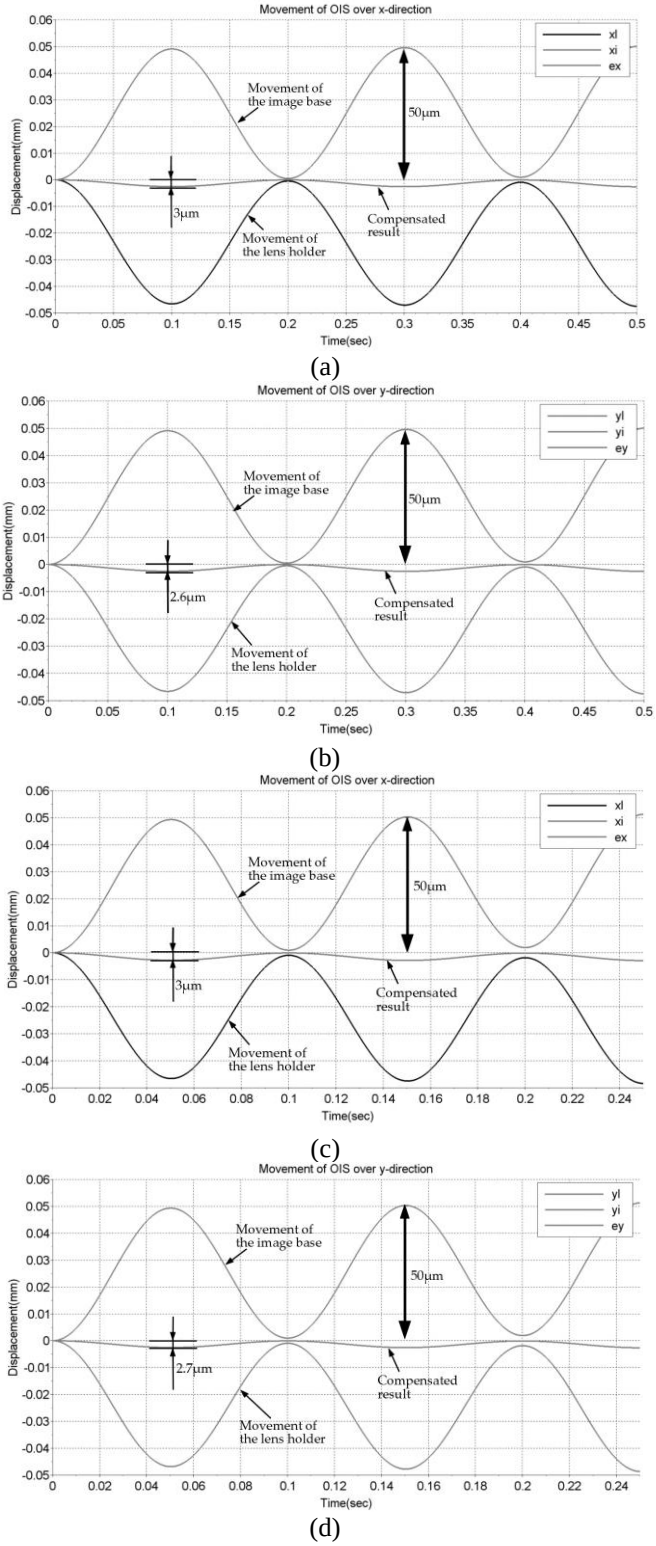

Figure 8. Simulated movements of the controlled the lens

holder relative to ground; (a) 5 Hz disturbance in 50 μm along x-axis. (b) 5 Hz disturbance in 50 μm along y-axis. (c) 10 Hz disturbance in 50 μm along x-axis. (d) 10 Hz disturbance in 50 μm along y-axis.

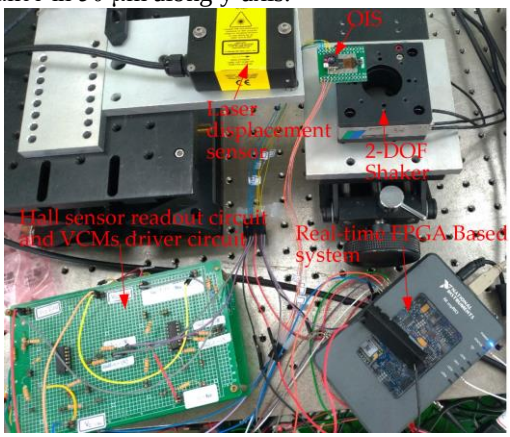

(a)

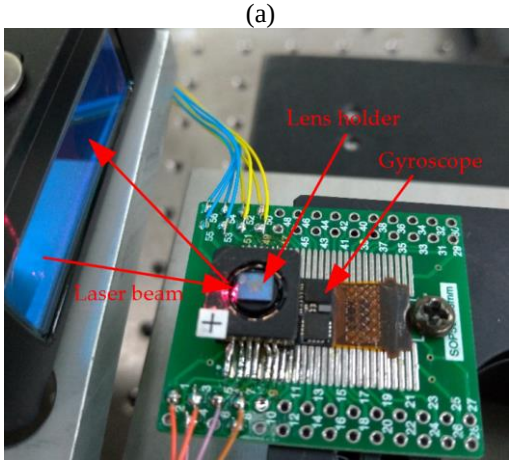

(b)

Figure 9. (a) Experimental setup; (b) the laser displacement sensor measures the motion of the lens holder.

VI. Conclusion

A compact OIS is designed and fabricated as a novel design that compensates external vibrations by the two-DOF translational mechanism. The OIS is satisfactory to fulfill requirements of a small and slim size and suitable to be installed in a cell phone. This study has accomplished several goals – mechanical analysis, the desired reference calculation, system identification, derivation and analysis of dynamic equations and the GA-based sliding mode controller design. After these steps, the GA-based SMC owns robustness and satisfactory performance to improve blurred images. Differential types of assumed shock are simulated for verified the GA-based SMC. The simulation results represent that the magnitudes of the observed shock on the lens holder have been reduced about of 3 μm, which are reduced to the 6 percent of the original shock, after the compensation. The experimental results show the compensated signal is reduced about 5 μm – 8 μm, which are attenuated the 10 - 16 percent of the original shock. The GA-based SMC can stabilize the lens holder within 0.05 seconds, which is faster than the earlier study with result of around 0.1 seconds. Obviously, OIS module is finally accomplished with satisfactory performance of vibration reduction. conclusion section is not required. Although a conclusion may review the main points of the paper, do not replicate the abstract as the conclusion. A conclusion might elaborate on the importance of the work or suggest applications and extensions.

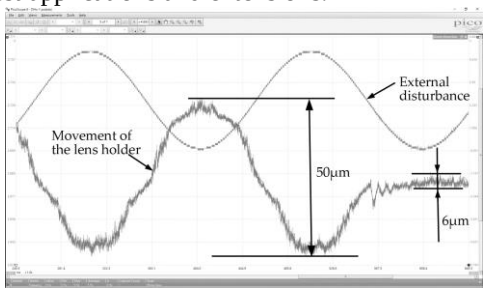

(a)

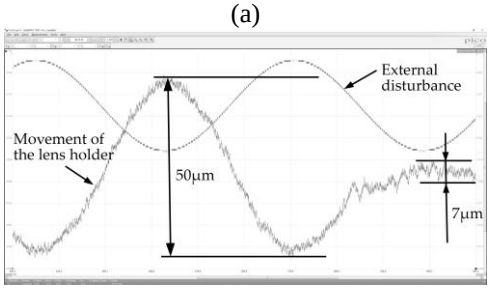

(b)

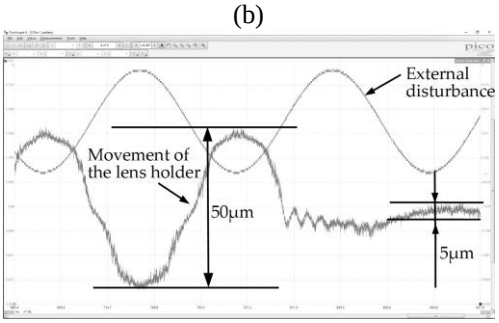

(c)

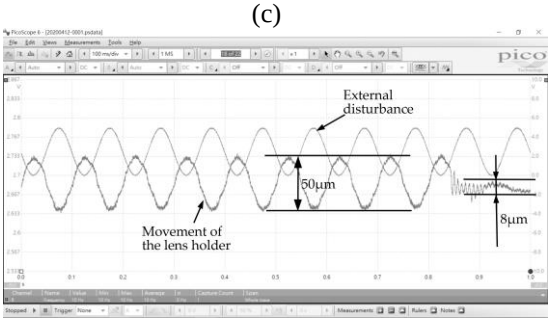

(d)

Figure 10. Experiments for the GA-based sliding mode controller are conducted under differential harmonic signals simulating the common hand shaking;(a)(b) 5 Hz disturbance in 50 μm along x- and y-axis, respectively; (c)(d) 10 Hz disturbance in 50 μm along x- and y-axis, respectively.

References

[1] S.-J. Ko, S.-H, Lee, K.-H. Lee, "Digital image stabilizing algorithms based on bit-plane matching," IEEE Trans. Consum. Electron. 1998, vol. 44, pp. 617-622.

[2] D.H. Yeom, "Optical image stabilizer for digital photographing apparatus," IEEE Trans. Consum. Electron. 2009, vol. 55, pp. 1028-1031.

[3] A. Gasteraos, "Active camera stabilization with fuzzy-grey controller," Eur. J. Mech Environ. Eng. 2009, vol. 2, pp. 18-20.

[4] J.-Y. Chang, W.-F. Hu, M.-H. Cheng, B.-S. Chang, "Digital image translational and rotational motion stabilization using optical low technique," IEEE Trans. Consum. Electron. 2002, vol. 48, pp. 108-115.

[5] H.-C. Yu, T.-Y. Lee, S.-K. Lin, L.-T. Kuo, S.-J. Wang, J.-J. Ju, D.-R. Huang, "Low power consumption focusing actuator for mini video camera," J. Appl. Phys. 2006, vol. 99, pp. 08R901-1-08R901-3.

[6] S.-J. Ko, S.-H. Lee, K.-H. Lee, "Digital image stabilizing algorithms based on bit-plane matching," IEEE Trans. Consum. Electron. 1998, vol. 44, pp. 617-622.
[7] K. Sato, S. Ishizuka, A. Nikami, M. Sato, "Control techniques for optical image stabilizing system," IEEE Trans. Consum. Electron. 1993, vol. 39, pp. 461-6466.
[8] H. Kusaka, Y. Tsuchida, T. Shimohata, "Control technology for optical image stabilization," SMPTE J. 2002, vol. 111, pp. 609-615.
[9] K. Nisshi, T. Onda, "Evaluation system for camera shake and image stabilizers," IEEE Int. Conf. on Multimedia and Expo (ICME), Singapore, 2010, pp.926-931.
[10] L.D. Landau, E.M. Lifshitz, *Mechanics*, 2nd ed., London: Pergamon Press:, 1969, pp. 126-129.
[11] Joel A. Shapiro, "Classsical Mechanics," unpublished, 2002, pp.94-97.
[12] Alain J. Brizard, "An introduction to Lagrangian mechanics," unpublished, 2007, pp. 139-143.
[13] F. La Rosa, M.C. Vizi, F. Bonaccorso, M. Branciforte, "Optical image stabilization (OIS)" Available online: http://www.st.com/resource/en/white_paper/ois_white_paper.pdf (accessed on 31 March 2020).
[14] ROHM Semiconductor, *Optical image stabilization (OIS)*, Available online: https://www.rohm.com/documents/1130/41217/OIS-white-paper.pdf (accessed on 31 March 2020)
[15] R.-G. Chi, L.-P. Chen, C.-G. Yang, M. Chen, "Extend state observer-based integral sliding mode control for an underwater robot with unknown disturbances and uncertain nonlinearities," IEEE Trans. Ind. Electron. 2017, vol. 64, pp. 6785-6795.
[16] S.-L. Jung, Y.-Y. Tzou, "Discrete sliding-mode control of a PWM inverter for sinusoidal output waveform synthesis with optimal sliding curve," IEEE Trans. Power Electron. 1996, vol. 11, pp. 567-577.
[17] H. O. Ozer, A. Sayin, N. Korkmaz, N. Yagiz, "Genetic algorithm integrated sliding mode control of a vehicle," 11th Congress on Computational Mechanics (WCCM XI) 2014, pp. 3857-3868.
[18] Frank H.F. Leung, H.K. Lam, S.H. Ling, Peter K. S. Tam, "Tuning of the structure and parameters of neural network using an improved genetic algorithm," IEEE Trans. Nerual Netw. 2003, vol. 14, pp. 79-88.
[19] E. Köse, K. Abacı, H. Kızmaz, S. Aksoy, M. A. Yalçin, "Sliding mode control based on genetic algorithm for WSCC systems include of SVC," Electronics and Electrical Engineering, 2013, vol. 19, pp. 25–28.
[20] C.-S. Chin, W. P. Lin, "Robust genetic algorithm and fuzzy inference mechanism embedded in a sliding-mode controller for an uncertain underwater robot," IEEE/ASME Trans. Mechatronics. 2018, vol. .23, pp. 655-666.
[21] Y. Zhang, "Sliding mode control with nonlinear disturbance observer based on genetic algorithm for rotary steering drilling stabilized platform," Res J Appl Sci Eng Tech. 2013, vol. 6, pp. 3187-3192.
[22] J. Wang, J.-P. Sheng, R.-Q. Gong, S.-Y. Jin, Y.-H. Xie, "Use Genetic algorithm to sliding mode control of active power filters." Int. Conf. on Computer Engineering and Information Systems, Shanghai, 2016, pp. 62-67.
[23] R.-J. Wai, C.-H. Tu, "Design of total sliding-mode-based genetic algorithm control for hybrid resonant-driven linear piezoelectric ceramic motor," IEEE Trans. Power Electron. 2007, vol. 22, pp. 563-575.
[24] G. Bartolini, "Chatter phenomena in discontinuous control systems," Int. J. Syst. Sci. 1989, vol. 20, pp. 2471-248.
[25] J.-J. Slotine, W.P. Li, *Applied nonlinear control*, 1st ed.; New Jersey :Prentice-Hall, 1991, pp. 123-126.
[26] G. J. Gray, Y. Li, D. J. Murray-Smith, K. C. Sharman, "Specification of a control system fitness function using constraints for genetic algorithm based design methods," Proc. First IEE/IEEE Int. Conf. on GA in Eng. Syst.: Innovations and Appl., Sheffield, UK, 1995, pp. 530-535.
[27] Joshua Waller. *Complete Guide to Image Sensor Pixel Size*. Available online: https://www.ephotozine.com/article/complete-guide-to-image-sensor-pixel-size-29652 (accessed on 31 March 2020).

Jeremy H.-S. Wang received the B.S. degree from National Taipei University of Technology, Taipei, Taiwan, R.O.C., in 1996 and the M.S. degree from National Cheng-Kung University, Tainan, Taiwan, R.O.C., in 2000. He is engaged in research on control technology.

Paul C.-P. Chao received the B.S. degree from National Cheng-Kung University, Tainan, Taiwan, R.O.C., in 1989 and the M.S. and Ph.D. degrees from Michigan State University, Lansing, in 1993 and 1997, respectively. After graduation, he worked for the CAE Department, Chrysler Corporation, Auburn Hill, MI, for two years. He is currently a Faculty Member of the Electrical and Control Engineering Department, National Chiao Tung University, Hsinchu, Taiwan. In recent years, his research interests focus on the electronics for optical systems; micro-mechatronics, control technology, micro- sensors, and actuators.